Downregulation of miR-7 and miR-153 is involved in *Helicobacter pylori* CagA induced gastric carcinogenesis and progression

YU SONG[1,2*], DONG GUO[1*], JIA-FEI LIU[1], LI-NA GE[1], PENG LIU[1], YE-MIN QU[1], HAI-YAN CONG[1], TIAN LI[3], XIN CHANG[1], YI-RAN WANG[4], LI-YING SHAO[1], ZONG-JUN DU[2] and MING-YI WANG[1]

[1]Department of Central Lab, Weihai Municipal Hospital, Cheeloo College of Medicine, Shandong University, Weihai, Shandong 264200; [2]Marie College, Shandong University, Weihai, Shandong 264209; [3]Department of Gastroenterology, Weihai Municipal Hospital, Weihai, Shandong 264200; [4]Department of Biomedical Sciences, City University of Hong Kong, Hong Kong, SAR 999077, P.R. China

Received November 19, 2022; Accepted April 26, 2023

DOI: 10.3892/ijo.2023.5527

Abstract. *Helicobacter pylori* (*H. pylori*) infection plays a pivotal role in the development of gastric cancer (GC). However, the association between aberrant microRNAs (miRNAs/miRs) expression and *H. pylori*-induced GC remains poorly understood. The present study reported that repeated infection of *H. pylori* caused the oncogenicity of GES-1 cells in BALB/c Nude mice. miRNA sequencing revealed that both miR-7 and miR-153 were significantly decreased in the cytotoxin-associated gene A (CagA) positive GC tissues and this was further confirmed in a chronic infection model of GES-1/HP cells. Further biological function experiments and *in vivo* experiments validated that miR-7 and miR-153 can promote apoptosis and autophagy, inhibit proliferation and inflammatory response in GES-1/HP cells. All the associations between miR-7/miR-153 and their potential targets were revealed via bioinformatics prediction and dual-luciferase reporter assay. Particularly, downregulation of both miR-7 and miR-153 obtained an improved sensitivity and specificity in diagnosing *H. pylori* (CagA+)-induced GC. The present study identified that the combination of miR-7 and miR-153 may be regarded as novel therapeutic targets in *H. pylori* CagA (+)-associated GC.

Correspondence to: Professor Ming-Yi Wang, Department of Central Lab, Weihai Municipal Hospital, Cheeloo College of Medicine, Shandong University, 70 Heping Road Weihai, Shandong 264200, P.R. China
E-mail: wangmingyi1973@outlook.com

*Contributed equally

Key words: Helicobacter pylori, cytotoxin-associated gene A, miR-7, miR-153, gastric cancer

Introduction

Gastric carcinoma (GC) is the third commonest cause of cancer death globally (1). Multiple risk factors, including gene polymorphism, dietary habits and smoking, have been reported as key factors in GC. However, *H. pylori* infection is known as the main risk, accounting for 90% of new cases of non-cardia gastric cancer (2). Growing evidence shows that *H. pylori* virulence factors have important roles in the carcinogenesis pattern 'chronic gastritis-gastric mucosa atrophy-intestinal metaplasia-dysplasia-gastric cancer' (3-5). Particularly, CagA is demonstrated to be the critical risk factor for chronic infection (6,7). It can interact with a variety of intracellular proteins, perturb multiple intracellular signaling pathways and promote the malignant transformation of the host cells (6). However, the molecular mechanism of *H. pylori* (CagA+)-induced GC is still not fully understood.

microRNAs (miRNAs/miRs) serve crucial roles in a variety of biological processes, including tumorigenesis and progression (8). Aberrant regulation of miRNAs can function as oncogenes or anti-oncogenes by binding with its specific target mRNAs, resulting in mRNA degradation or/and translational repression (9). Studies have revealed the regulatory roles of miRNAs in *H. pylori*-induced inflammation and carcinogenesis (10-13).

As an ancient miRNA, miR-7 is involved in the fine-tuning of several signaling pathways, serving primarily as a tumor suppressor in various cancers (14). It can suppress tumor metastasis via neuro-oncological ventral antigen 2 (NOVA2) in non-small cell lung cancer (15), suppress the progression of pancreatic cancer via mitogen-activated protein kinase kinase 9 (MAP3K9) (16) and reduce breast cancer stem cell metastasis by suppressing RELA proto-oncogene, NF-κB subunit (RELA) and decreasing the expression of endothelial cell-selective adhesion molecule (ESAM) (17). miR-7 is downregulated in GC (18); it can inhibit proliferation and angiogenesis and promotes apoptosis of GC cells via Raf-1 (19), increase cisplatin sensitivity of GC cells through suppressing mTOR (20), inhibit the invasion and metastasis

of GC cells through inhibitions of EGFR (21) and insulin-like growth factor-1 receptor (IGF1R) (22). Particularly, it can form a regulatory feedback circuit with NF-κB (23) and act as a potential therapeutic target for aberrant NF-κB-driven distant metastasis of GC (24).

miR-153 exerts opposite functions as a tumor promoter or suppressor in different types of cancer. It can improve sensitivity to gefitinib by regulating the expression of ABCE1 in lung cancer (25), inhibit triple-negative breast cancer by targeting zine finger E-box-binding homeobox2 (ZEB2)-induced epithelial-mesenchymal transition (EMT) (26), regulate the progression of ovarian carcinoma by targeting myeloid cell leukemia 1 (MCL1) (27) and decrease tryptophan catabolism and inhibit angiogenesis via the repression of indoleamine 2,3-dioxygenase 1 in bladder cancer (28). Meanwhile, high expression of miR-153 is relevant for a poor prognosis for prostate cancer patients (29). miR-153 also increases invasion and therapeutic resistance by pleiotropic effects in colorectal cancer progression (30). Nevertheless, relevant studies of miR-153 in GC are rare. miR-153 acts as a tumor suppressor by aiming at Krüppel-like factor 5 (KLF5) in GC (31).

To date, the synergistic roles of miRNAs have not been well elucidated in GC. In the present study, an integrated approach was adopted and identified that miR-7 and miR-153 were involved in *H. pylori*-induced gastric carcinogenesis and progression. The present study systematically validated that simultaneous overexpression of miR-7 and miR-153 significantly promoted apoptosis, inhibited proliferation and inflammatory response by multiple targets. In addition, it was discovered that a combination of miR-7 and miR-153 might serve as novel diagnostic and therapeutic targets in *H. pylori* CagA (+)-associated GC.

Materials and methods

Cell lines, bacterial strains and culture. Human normal gastric epithelial cell line GES-1(RRID:CVCL_EQ22) and human GC cell lines MKN-45 (RRID:CVCL_0434), MKN-28 (RRID:CVCL_1416), HGC-27 (RRID:CVCL_1279), SNU-1 (RRID:CVCL_0099) and AGS (RRID:CVCL_0139) were purchased from the BeNa Culture Collection. GC cell line NCL-87 was purchased from the National Collection of Authenticated Cell Cultures. Cell lines were cultured in RPMI-1640 medium (HyClone; Cytiva) and maintained in a humidified atmosphere containing 5% CO_2 at 37˚C. All cell cultures were supplemented with 10% fetal bovine serum (FBS; Biological Industries), 100 IU/ml penicillin and 100 μg/ml streptomycin (Gibco, Thermo Fisher Scientific, Inc.).

H. pylori clinical isolate SBK was isolated from a gastric ulcer patient and preserved in Central Lab of Weihai Municipal Hospital. CagA-knockout *H. pylori* SBK was established according to the previously described method (32). *H. pylori* strain ATCC 26695 and its corresponding CagA-knockout *H. pylori* (named 0547) were kindly provided by Professor Boqing Li of Binzhou Medical University (Yantai, China). All strains were maintained in Colombian agar plates supplemented with 8% sheep blood under a microaerophilic environment.

Cell chronic infection model. GES-1 cells were co-cultured with *H. pylori* strain ATCC 26695 or isolated SBK at a multiplicity of infection (MOI) of 100:1 to construct the *H. pylori* chronic infection model, as previously described (33). However, only the SBK-treated GES-1 survived and was termed GES-1/HP. GES-1cells without exposure to *H. pylori* underwent the same procedure and were designated as control cells.

Construction and sequencing of miRNA libraries. High-throughput sequencing was performed to identify miRNAs as follows: steps. Total RNA isolated from *H. pylori*-infected GC tissues and paired adjacent normal tissues were fractionated with a 15% native polyacrylamide gel (Invitrogen; Thermo Fisher Scientific, Inc.) and small RNAs of 18-30 nt were purified. Small RNAs were reverse transcribed into cDNA and further amplified. The sequence of the amplified products was performed on the Illumina HiSeq 2500 platform (Guangzhou RiboBio Co., Ltd.).

miRNA/RNA extraction and reverse transcription-quantitative (RT-q) PCR. Total miRNAs or RNA were extracted from $1x10^7$ cells with RNAiso for Small RNA or RNAiso Plus (Takara Bio, Inc.) according to the manufacturer's protocol, and the concentrations were measured with the NanoDrop ND-1000 spectrophotometer (Thermo Fisher Scientific, Inc.). Then, 1-3 μg miRNA or RNA was reverse transcribed. RT-qPCR was performed using TB Green Premix Ex Taq II (Takara Biotechnology Co., Ltd.) on the 7500 Real-Time PCR instrument (Thermo Fisher Scientific, Inc.) according to the manufacturer's instructions. U6 small nuclear RNA and β-actin were used as an internal control for miRNA and mRNA assays, respectively. Specific primers used for SP1, Bcl-xL, Bcl2, β-actin, miR-7, miR-153 and U6 were as follows: 5'-CCTCAGTGCATTGGGTACTTC (forward) and 5'-ACCAAGCTGAGCTCCATGAT (reverse) for SP1; 5'-GAGCTGGTGGTTGACTTTCTC (forward) and 5'-TCCATCTCCGATTCAGTCCCT (reverse) for Bcl-xL; 5'-GGTGGGGTCATGTGTGTGG (forward) and 5'-CGG TTCAGGTACTCAGTCATCC (reverse) for Bcl2; 5'-CAT GTACGTTGCTATCCAGGC (forward) and 5'CTCCTTAAT GTCACGCACGAT-(reverse) for β-actin; 5'-CCACGTTGG AAGACTAGTGATTT (forward) and 5'TATGGTTTTGAC GACTGTGTGAT-(reverse) for miR-7; 5'-AACGAACTTGCA TAGTCACAAAAG (forward) and 5'TATGGTTTTGACGAC TGTGTGAT-(reverse) for miR-153; 5'-CAGCACATATAC TAAAATTGGAACG (forward) and 5'ACGAATTTGCGT GTCATCC-(reverse) for U6. Fold changes of target miRNAs or genes were calculated by the $2^{-\Delta\Delta Cq}$ method from triplicate experiments (34).

Western blotting. Cells or tissue samples were collected and lysed with T-PER (Thermo Fisher, Inc.) containing protease inhibitor and phosphatase inhibitor cocktail (Biotool, LLC), then incubated 30 min on ice and centrifuged at 13,700 x g at 4˚C for 15 min. The supernatants were collected carefully and determined by BCA protein concentration assay kit (Beyotime Institute of Biotechnology). Total proteins (30 μg) were separated by 10% SDS-PAGE. Gels were transferred onto PVDF membranes by wet transfer. Membranes were blocked in 5% BSA in TBST (20 mM Tris-HCl, 150 mM NaCl, 0.05%

Tween-20, pH 8.0) at 37˚C for 2 h, incubated with primary antibodies to Bax (1:1,000; cat. no. 5023), Bcl-xL (1:1,000; cat. no. 2764), Bcl-2 (1:1,000; cat. no. 15071), Cleaved Caspase-3 (1:1,000; cat. no. 9661), phosphorylated (p)-AKT (cat. no. 4060), IL-1β (1:1,000; cat. no. 12703S) and AKT (1:1,000; cat. no. 4685; Cell Signaling Technology, Inc.); P53 (1:1,000; cat. no. 60283-2-Ig), P27 (1:1,000; cat. no. 25614-1-AP), SP1 (1:1,000; cat. no. 21962-1-AP), Cyclin A2 (1:1,000; cat. no. 66391-1-Ig), Cyclin E2 (1:1,000; cat. no. 11935-1-AP), Toll-like receptor 4 (TLR4; 1:1,000; cat. no. 19811-1-AP), Krüppel-like factor (KLF)5 (1:1,000; cat. no. 21017-1-AP; Proteintech Group, Inc.) and Ki-67 (1:1,000; cat. no. AF1738) and NF-κB p65 (1:1,000; cat. no. AF0246; Beyotime Institute of Biotechnology) overnight at 4˚C, and then incubated with appropriate HRP-conjugated secondary antibody (1:5,000; cat. nos. A0208 or A0216; Beyotime) at room temperature for 30 min. Finally, the specific bands were visualized using super sensitive ECL chemiluminescence detection reagent (Tiangen Biotech Co., Ltd.) and imaged with Chemidoc XRS+ (Bio-Rad Laboratories, Inc.).

Cell apoptosis assay. This was performed according to the manufacturer's protocol as described previously (33). Briefly, cells were harvested, resuspended and labelled using an Annexin V-FITC apoptosis detection kit (BD Biosciences). Then, cells were analyzed by flow cytometer BD FACSaria II (BD Biosciences), and the total percentage of early + late apoptotic cells were processed for the apoptotic rate using the CellQuest Pro software v8.0.1 (BD Biosciences).

EdU assay. This was performed in accordance with the manufacturer's protocol using the BeyoClick EdU Cell Proliferation kit with Alexa Fluor 488 (Beyotime Institute of Biotechnology). In brief, cells were incubated with 10 μM EdU reagent at 37˚C for 2 h, fixed with 4% paraformaldehyde for 15 min and permeated with 0.3% Triton X-100 for another 15 min at room temperature. The cells were incubated with the Click Reaction Mixture at room temperature for 30 min and then incubated with Hoechst 33342 for 10 min in a dark place. The ratio of EdU-positive cells to the total number of Hoechst 33342-positive cells was calculated as the cell proliferation rate.

Cell transfection. GES-1/HP cells and HGC-27 cells under *H. pylori* infection ($5x10^5$ cells/well) were transfected with miR-7-5p mimics (50 nmol; cat. no. miR1181031074037-1-5), miR-153-3p mimics (50 nmol; cat. no. miR10000439-1-5), combination of miR-7-5p (25 nmol) and miR-153-3p mimics (25 nmol), mimics negative control (NC, 50 nmol; cat. no. miR1N0000001-1-5; Guangzhou RiboBio Co., Ltd.), SP1 short interfering (si)RNA (cat. no. A10001) and negative control siRNA (cat. no. A06001; Shanghai GenePharma Co., Ltd.) in 6-well plates using the Lipofectamine 2000® (Invitrogen; Thermo Fisher Scientific, Inc.) according to the manufacturer's protocol at 37˚C for 6 h. The sequences of validated siRNA for SP1 were: 5'-CCAGCAACAUGGGAAUUAUTT (forward) and 5'-AUAAUUCCCAUGUUGCUGGTT (reverse) for si-1; 5'-GCCGUUGGCUAUAGCAAAUTT (forward) and 5'-AUU UGCUAUAGCCTTAACGGCTT (reverse) for si-2; 5'-GCC CUUAUUACCACCAAUATT (forward) and 5'-UAUUGG UGGUAAUAAGGGCTT (reverse) for si-3; the sequences of negative control were 5'-UUCUCCGAACGUGUCACGUTT (forward) and 5'-ACGUGACACGUUCGGAGAATT (reverse). The time interval between transfection and subsequent experimentation was 48 h.

Dual-luciferase reporter assay. Bcl-xL-3'-UTR/wild-type (WT), Bcl-xL-3'-UTR/mutant (MUT), Bcl2-3'-UTR/WT and Bcl2-3'-UTR/Mut were cloned and embedded into the psiCHECK-2 plasmid. Cells were co-transfected with either WT or MUT luciferase reporter vector and either mimic miRNAs or negative control using Lipofectamine 2000® (Invitrogen; Thermo Fisher Scientific, Inc.), respectively. After 48 h transfection, cells were treated using Dual-Luciferase Reporter Gene Assay kit (Beyotime Institute of Biotechnology). Dual fluorescent signals were detected with a luminometer (GloMax Navigator; Promega Corporation) and each value for Renilla luciferase activity was normalized by firefly luciferase activity.

Cell cycle assay. The cell cycle assay was conducted using a cell cycle and apoptosis kit (Beyotime Institute of Biotechnology) according to the manufacturer's protocol. Cells transfected with miR-7, miR-153 or miR-7 and miR-153 together at 37˚C for 48 h were digested and stained with propidium iodide at 37˚C for 30 min in the dark. Then, the cell DNA content was determined by the flow cytometer BD FACSaria II (BD Biosciences), and the cell cycle was analyzed using the FlowJo software (v10.8.2; FlowJo LLC).

Fluorescence in situ hybridization (FISH) analysis. A FAM-labeled Locked Nucleic Acid (LNA) probe for detecting miR-7 and a Cy3-labeled LNA probe for detecting miR-153 were synthesized and performed on paraffin sections using a fluorescence in situ hybridization kit (Shanghai GenePharma Co., Ltd.). In brief, firstly, the dissected tissues were fixed with 10% formalin for 48 h at room temperature. After rinsing the tissues with running tap water and dehydrating the tissues in EtOH baths at 70, 95 and 100% ethanol, successively, the tissues were incubated in a 65˚C paraffin bath twice, 30 min each. Then, the paraffin-embedded tissues were sectioned at 4 μm. Subsequently, the paraffin sections were dewaxed, rehydrated, digested with proteinase K at 37˚C for 20 min, and dehydrated through a graded series of alcohol. Then, the sections were hybridized with the probes directed against miR-7 and miR-153 at 37˚C for overnight in wet box, and further counterstained with 4,6-diamidino-2-phenylindole (DAPI) at room temperature for 10 min. Images were captured using fluorescence microscopy (Nikon Corporation).

Immunohistochemical (IHC) analysis. Paraffin sections were made from *H. pylori*-infected GC tissues, adjacent normal tissues and xenograft tumor samples according the following steps: First, the dissected tissues were fixed with 10% formalin for 48 h at room temperature. After rinsing the tissues with running tap water and dehydrating the tissues in EtOH baths in the 70, 95 and 100% ethanol, successively, the tissues were incubated in a 65˚C paraffin bath twice, 30 min each. Then, the paraffin-embedded tissues were sectioned at 4 μm. The paraffin sections were dewaxed and underwent antigen retrieval

with citrate buffer. The slides were blocked with 0.1% BSA and incubated overnight with the following antibodies: Bcl-xL (1:50; cat. no. 2764; Cell Signaling Technology, Inc.), Bcl-2 (1:50; cat. no. 15071; Cell Signaling Technology, Inc.), Ki-67 (1:100; cat. no. AF1738; Beyotime Institute of Biotechnology), SP1 (1:50; cat. no. 21962-1-AP; Proteintech Group, Inc.) or P53 (1:100; cat. no. 60283-2-Ig) at 4˚C overnight, and then incubated with HRP-conjugated secondary antibodies (1:50; Beyotime Institute of Biotechnology) at 37˚C for 1 h. Finally, the target proteins were visualized on-site with the 3,3'-diaminobenzidine substrate (Beyotime Institute of Biotechnology) and images captured using fluorescence microscopy (Nikon Corporation).

Chromatin immunoprecipitation (ChIP). ChIP assay was conducted following the instructions of the ChIP Assay kit (Beyotime Institute of Biotechnology). Briefly, cultured cells ($1x10^7$ cells in 10 cm dish) were fixed with 1% formaldehyde at 37˚C for 10 min, and then neutralized with 125 mM glycine solution (1.1 ml) at room temperature for 5 min. Chromatin solutions were sonicated and incubated with anti-SP1 antibody (1:100) or control IgG (1:100) overnight with rotation at 4˚C. DNA-protein cross-links were disassembled and chromatin DNA was purified and subjected to PCR analysis with the primers: 5'-CCGCTCGAGCGGCCAGGTCGGCGAGAATCCT-3' and 5'-CCCAAGCTTGGGTTAGCGCCAGTCTTGAGCACAT-3' for SP1, 5'-TACTAGCGGTTTTACGGGCG-3' and 5'-TCGAACAGGAGGAGCAGAGAGCGA-3' for *GAPDH* as a negative control. DNA isolated from total nuclear extract was used the PCR input control, and the PCR products were analyzed by gel electrophoresis using a 2% agarose gel. PrimeSTAR HS DNA Polymerase (Takara Bio Inc.) was used for the PCR process. Thermocycling conditions was initial denaturation: 98˚C for 5 min; 30 cycles of denaturation (98˚C for 10 sec), annealing (60˚C for 15 sec) and elongation (72˚C for 15 sec).

Nude mouse tumor xenograft model. A total of 20 Balb/c male nude mice, 4-6 weeks old, weighing 20-25 g, were obtained from Weihai Desheng Technology Testing Co., Ltd. and housed in standard pathogen-free conditions environment with a temperature of 22±1˚C, relative humidity of 50±1% and a 12-h light/dark cycle. All animal studies (including the mouse euthanasia procedure) were approved by the Ethics Committee of Weihai Municipal Hospital (approval no. 20220103) and conducted in compliance with the regulations and guidelines of Weihai Municipal Hospital institutional animal care and conducted according to the AAALAC and the IACUC guidelines.

To establish a xenograft model, $1x10^7$ HGC-27 cells were suspended in 100 μl PBS and inoculated subcutaneously into the right hind flank. After 2 weeks, the transplanted nude mice were randomly divided into three groups (n=5/group): i) MicrON hsa-miR-7 (cat. no. miR4180703093100-4-5; Guangzhou RiboBio Co., Ltd.), ii) micrON hsa-miR-153 (cat. no. miR40000439; Guangzhou RiboBio Co., Ltd.) and iii) MicrON hsa-miR-7 and micrON hsa-miR-153 together were injected into the unilateral implanted tumor at the dose of 5 nmol (in 20 μl PBS) per mouse under anesthesia with isoflurane inhalation (2-3% induction, 1-2% maintenance). The implanted tumor on the other side was injected with micrON agomir NC#22 (cat. no. miR4N0000001-2-5; Guangzhou RiboBio Co., Ltd.) as NC. Tumor volume were calculated as $\pi/6$ x width^2 x length every 4 days for 5 times. After 6 weeks, mice were euthanized by cervical dislocation under anesthesia (1% sodium pentobarbital intraperitoneal injection, 30 mg/kg) and tumor tissues were excised, measured, weighed and used for IHC and FISH. The mice were euthanized when reaching the following humane endpoints: i) Tumor burden was >10% of body weight and the diameter of tumor was >20 mm; ii) tumor ulceration, infection or necrosis was observed; iii) tumor interferes with eating or walking; iv) rapid weight loss (loss of 15-20% of original weight). Notably, none of these endpoints were reached during the experiments. Animal health and behavior were monitored twice a day (at the beginning and end of the day) by an experienced individual. A comprehensive judgment on death was made by observing cessation of respiration, heartbeat and pupil and nerve reflexes.

IL-1β levels quantification (ELISA). IL-1β levels in GES-1 cells treated with or without *H. pylori* infection and biopsy specimens obtained from the antrum of gastric patients with *H. pylori* infection and matched normal tissues were determined in duplicated samples by an ELISA (cat. no. PI305; Beyotime Institute of Biotechnology). Briefly, biopsy samples were immediately placed in 2 ml of PBS (pH 7.4), frozen on dry ice, homogenized and centrifuged (10,000 x g, 4˚C for 10 min). Then, total protein in supernatants or cell culture supernatants was measured and IL-1β levels were analyzed according to the manufacturer's instructions.

Patient samples. All blood and paired samples of *H. pylori*-infected GC tissues and adjacent normal tissues were obtained from Weihai Municipal Hospital. All samples were clinically and pathologically confirmed.

Tissue microarray analysis. GC tissue microarrays (TMAs) consisting of 24 cases of gastric disease (including six cases of GC tissue with matched adjacent normal gastric tissue) were obtained from Shanghai Outdo Biotech Co., Ltd. FISH probes and specific antibodies or were applied to slides followed the protocol of IHC and FISH described previously. Slides were scanned with a confocal scanner and images captured under fluorescence microscopy (Nikon Corporation). The staining intensity of TMAs was evaluated and scored using Image-Pro Plus 6.0 (Media Cybernetics, Inc.).

Bioinformation analysis. TargetScan (https://www.targetscan.org/vert_80/), miRDB (https://mirdb.org/) and picTar (https://pictar.mdc-berlin.de/cgi-bin/PicTar_vertebrate.cgi) are widely applicable to predict biological targets of miRNAs. In this study, we used TargetScan, miRDB and picTar to synthetically analyzed the targets of miR-7 or miR-153. Pathway Commons (http://www.pathwaycommons.org/) is a web resource for biological pathway data. The present study used Pathway Commons to analyzed the interaction between Sp1 and p53.

Statistical analysis. For the majority of experiments, the two-tailed, unpaired, Student's test was applied to compare groups. For paired GC and adjacent non-tumor tissues, the

two-tailed, paired, Student's test was used (GraphPad Prism V. 7.0 software; Dotmatics). Comparisons among multiple groups were analyzed using one-way ANOVA followed by Dunnett's post hoc test. Pearson correlation analysis was used to analyze correlation of two indexes. Data are presented as mean ± SD. P-values <0.05 was considered significant. receiver operating characteristic curve was introduced for assessing the diagnostic potential of miR-7, miR-153 and their combine in GC via Statistical Product and Service Solutions (SPSS) 22.0 (IBM, Armonk, NY, USA).

Results

miR-7 and miR-153 were downregulated in H. pylori-associated GC. Expression profile changes of miRNAs were analyzed between *H. pylori*-infected GC tissues and compared adjacent normal tissues using the Illumina HisSeq 2500 high-throughput sequencing (miRNA-seq) technique. A total of 331 miRNAs (159 upregulated and 172 downregulated, Table SI) were identified after fold change filtering and illustrated with hierarchical clustering analysis, scatter plots and volcano plots (Fig. 1A-C), respectively. Partially differently expressed miRNAs were further confirmed in our established chronic *H. pylori*-infected model GES-1/HP cells (Fig. 1D). Notably, both miR-153 and miR-7 were found to be significantly downregulated in *H. pylori* infected GC tissues and GES-1/HP cells, revealing that dysregulation of miR-7 and miR-153 is not only involved in *H. pylori*-induced gastric malt lymphoma (13).

CagA plays an important role on miRNA expression (35). To clarify the effect of CagA on the downregulation of miR-7 and miR-153, GES-1 cells were co-cultured with *H. pylori* strain 26695 and its corresponding CagA knockout strain 0547 with or without the addition of recombinant protein CagA, respectively. The results showed that infection of *H. pylori* strain 26695 significantly decreased the expression of miR-7 and miR-153 in GES-1 cells. Meanwhile, compared with infection of *H. pylori* strain 26695, a clear elevation was found in expression of miR-7 and miR-153 accompanied by knockout of CagA. The expression of miR-7 and miR-153 was further weakened with the addition of recombinant protein CagA, indicating that CagA might account for the downregulation of miR-7 and miR-153 (Fig. 1E). Subsequently, miR-7 and miR-153 were analyzed in GES-1 cells, GC cell lines and GES-1/HP cells and the results showed that miR-7 and miR-153 were both downregulated (Fig. 1F and G). The lower expression of miR-7 and miR-153 was confirmed by FISH analysis in *H. pylori*-infected GC tissues compared with adjacent normal tissues (Fig. 1H).

miR-7 and miR-153 combination significantly accelerates apoptosis and autophagy in H. pylori-associated GC cells. Numerous miRNAs regulate programmed cell death including apoptosis, autophagy and necroptosis. Particularly, some miRNAs serve important roles in crosstalk between apoptosis and autophagy. Our previous results demonstrated that apoptosis was inhibited in GES-1/HP cells. Some critical apoptosis-related proteins significantly changed, e.g., Bcl-xL, Bcl2 and P65 were significantly increased, while Bax and cleaved caspase-3 were decreased (33). Furthermore, as shown in Fig. 2A, an obvious increase in apoptosis was found when GES-1 cells were treated with SBK/ΔCagA. Western blotting showed that Bax and cleaved caspase-3 were enhanced in these cells (Fig. 2B).

To clarify the functional role of miR-7 and miR-153 on cell apoptosis, miR-7, miR-153, or their combination were overexpressed in GES-1/HP and *H. pylori*-infected HGC-27 cells (Fig. S1), respectively. As shown in Figs. 2C and D and S2A, miR-7 or miR-153 enhanced the apoptosis of the above cells. Western blotting showed that Bcl-xL and Bcl2 were more repressed, while Bax and cleaved caspase-3 were more upregulated in cells co-expressing both miR-7 and miR-153 compared to those overexpressing miR-7 or miR-153 alone (Figs. 2E and S2E). Moreover, it was found that autophagy marker Atg5 and LC3B increased with overexpression of miR-7 and miR-153 (Figs. 2E and S2E), consistent with previous reports (36,37). Collectively, these results demonstrated that miR-7 and miR-153 serve important roles in the crosstalk between apoptosis and autophagy.

Subsequently, bioinformatics algorithms (including TargetScan, miRDB and PicTar) indicated that there was a potential binding site of miR-7 in 3'UTR of Bcl-xL and a potential binding site of miR-153 in 3'UTR of Bcl2 (Fig. 2F and G, left). Dual-luciferase reporter assay showed that overexpression of miR-7 or miR-153 inhibited luciferase activity in Bcl-xL-w3'UTR reporter gene constructs or BCL-2-w3'UTR reporter gene constructs, respectively, but did not affect mutation reporter gene constructs (right of Fig. 2F and G, right). These results proved that Bcl-xL was a direct target of miR-7 and BCL-2 was a direct target of miR-153 in *H. pylori*-associated GC cells.

Combination of miR-7 and miR-153 significantly represses the proliferation of H. pylori-associated GC cells. Furthermore, the effects of miR-7 and miR-153 on cell proliferation were determined in GES-1/HP and *H. pylori*-infected HGC-27 cells, respectively. The results of EdU assay (Figs. 3A and S2B) and clone formation assay (Figs. 3B and S2C) confirmed that cell growth and proliferation ability were decreased with overexpression of miR-7, miR-153, or their combination. Western blotting results showed that the expression of p-AKT was significantly downregulated. Meanwhile, cell-cycle associated protein P53 and P27 were significantly upregulated when GES-1/HP and *H. pylori*-infected HGC-27 cells were overexpressed with miR-7, miR-153, or their combination (Figs. 3C and S2E). Cell cycle detection also showed that overexpression of miR-7, miR-153, or their combination could induce G_1 phase arrest (Figs. 3D and S2D).

In the xenograft model, miR-7 or miR-153 significantly reduced tumor volumes and weights and the miR-7 and miR-153 combination group had a much greater inhibitory effect than miR-7 or miR-153 alone (Fig. 3E and F). IHC analysis revealed that miR-7, or miR-153, or miR-7 and miR-153 treatment reduced proliferation via P53 and P27 (Fig. 3G).

miR-7 induces cell cycle arrest in H. pylori-associated GC cells via the Sp1/p53 axis. Bioinformatics algorithms and Pathway Commons (http://www.pathwaycommons.org/) implied that miR-7 might induce cell cycle arrest via the Sp1/p53 axis. Bioinformatics algorithms (including

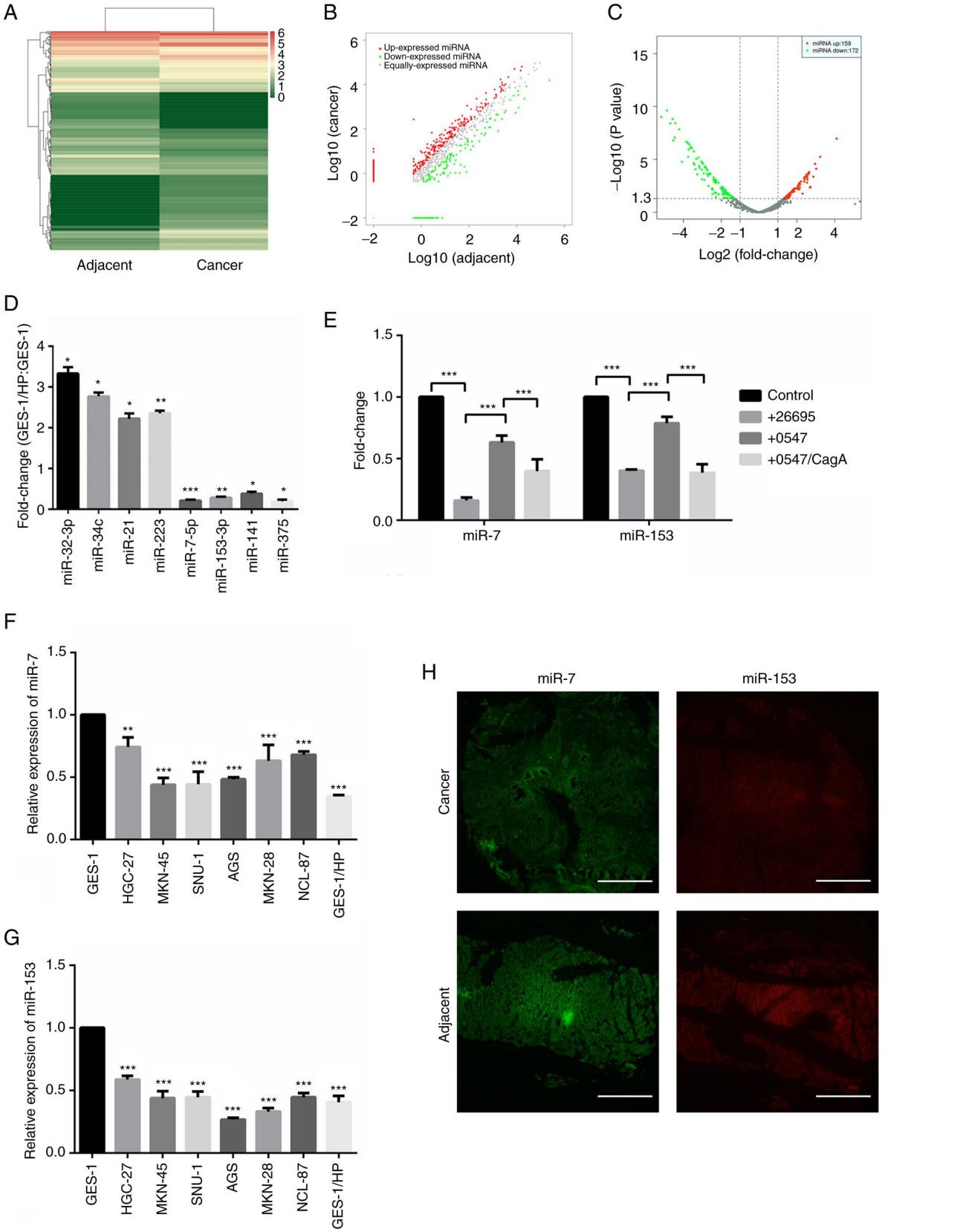

Figure 1. miR-7 and miR-153 are downregulated in *H. pylori*-associated GC. (A) Representative heatmap of differential expression levels of miRNAs in *H. pylori* (+) gastric cancer tissues compared with adjacent normal tissues obtained by sequencing on the Illumina HiSeq 2500 platform. (B) Scatter plots used to evaluate differences in the expression of miRNAs. (C) Volcano plot indicating differential expression. P≤0.05 and fold change ≥2 were considered statistically significant. (D) Partial upregulated and downregulated miRNAs validated by RT-qPCR. *P<0.05, **P<0.01, ***P<0.001. (E) Fold changes of miR-7 and miR-153 detected with RT-qPCR under treatment with *H. pylori* 26695 and 0547 with or without the addition of the recombinant protein CagA. ***P<0.001. (F) Relative expression of miR-7 was detected in GES-1, GC cells and GES-1/HP cells by RT-qPCR. ***P<0.001. (G) Relative expression of miR-153 detected in GES-1, GC cells and GES-1/HP cells by RT-qPCR. ***P<0.001. (H) Differential expressions of miR-7 and miR-153 were detected in *H. pylori*-infected GC tissues and adjacent normal tissues by fluorescence *in situ* hybridization. Scale bar, 500 μm. *H. pylori*, *Helicobacter pylori*; GC, gastric cancer; miRNA/miR, microRNA; RT-qPCR, reverse transcription-quantitative PCR; CagA, cytotoxin-associated gene A.

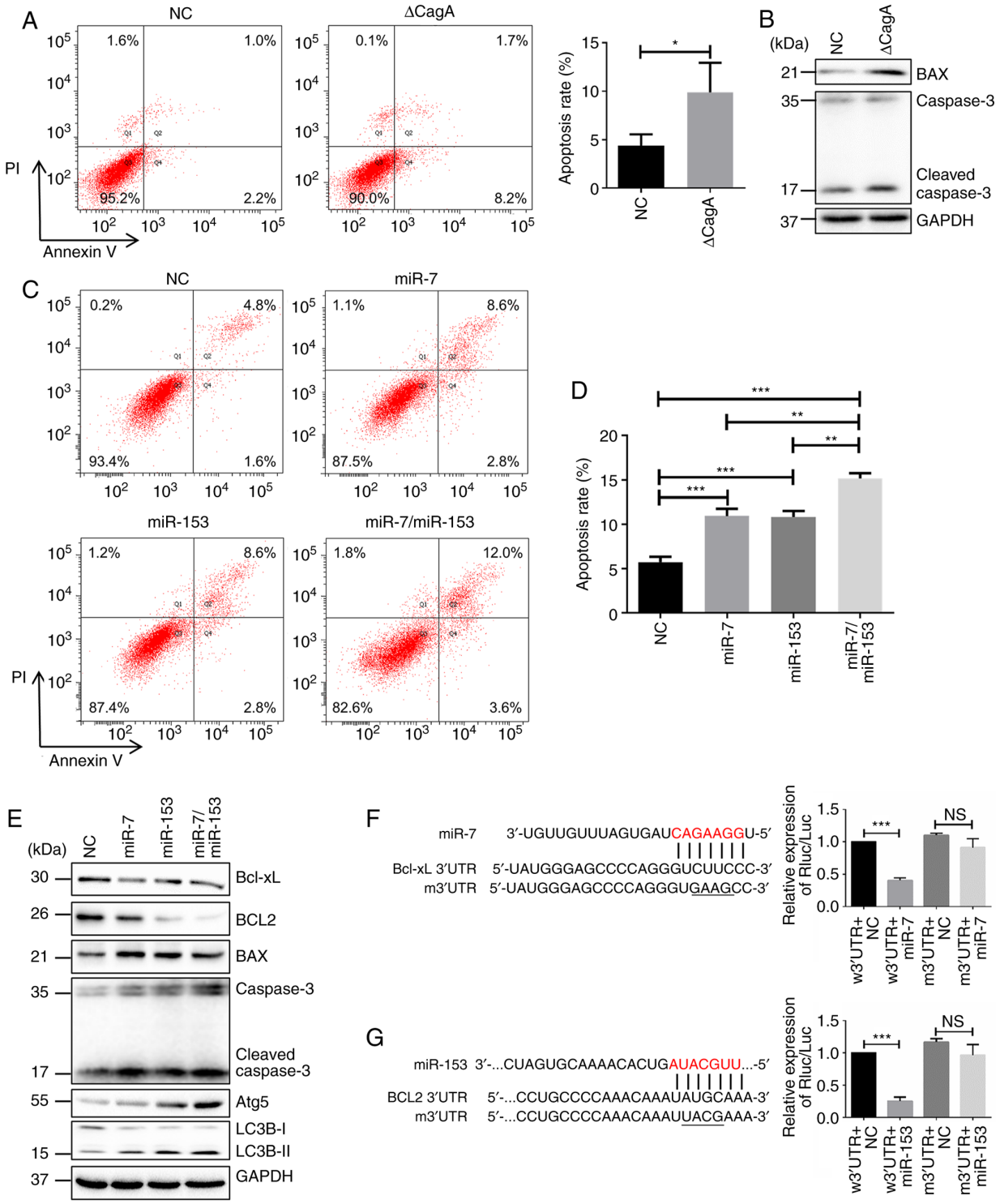

Figure 2. miR-7 and miR-153 significantly accelerates apoptosis of *H. pylori*-associated GC cells. (A) Apoptosis changes detected by flow cytometry in GES-1 cells following CagA knockdown in *H. pylori* SBK strain. *P<0.05. (B) Changes of apoptosis protein determined by western blotting. (C and D) Apoptosis changes detected in flow cytometry when miR-7, miR-153 or their combination overexpressed in GES-1/HP cells compared with NC. *P<0.05, **P<0.01, ***P<0.001. (E) Changes of apoptosis and autophagy related protein determined by western blotting. (F) Left: Putative miR-7 binding sites on 3'-UTR of Bcl-xL and the site discrepancies between wild-type and mutant type; right: GES-1/HP cells co-transfected with miR-7 mimic or mimic-NC and constructed reporter plasmids and relative luciferase activities were detected. ***P<0.001, NS, not significant. (G) Left: Putative miR-153 binding sites on 3'-UTR of Bcl2 and the site discrepancies between wild-type and mutant type; right: GES-1/HP cells co-transfected with miR-153 mimic or mimic-NC and constructed reporter plasmids and relative luciferase activities of transfected cells were detected. ***P<0.001, NS, not significant. miRNA/miR, microRNA; *H. pylori*, *Helicobacter pylori*; GC, gastric cancer; NC, negative control; w3'UTR, wild-type; m3'UTR, mutant.

TargetScan, miRDB and PicTar) indicated a potential binding site in 3'UTR of Sp1 (Fig. 4A). Dual-luciferase reporter assay was performed in GES-1/HP cells and the result showed that miR-7 overexpression inhibited luciferase activity in Sp1-wild-type (w)3'UTR reporter gene constructs, but did not affect Sp1-mutant (m)3'UTR reporter gene constructs

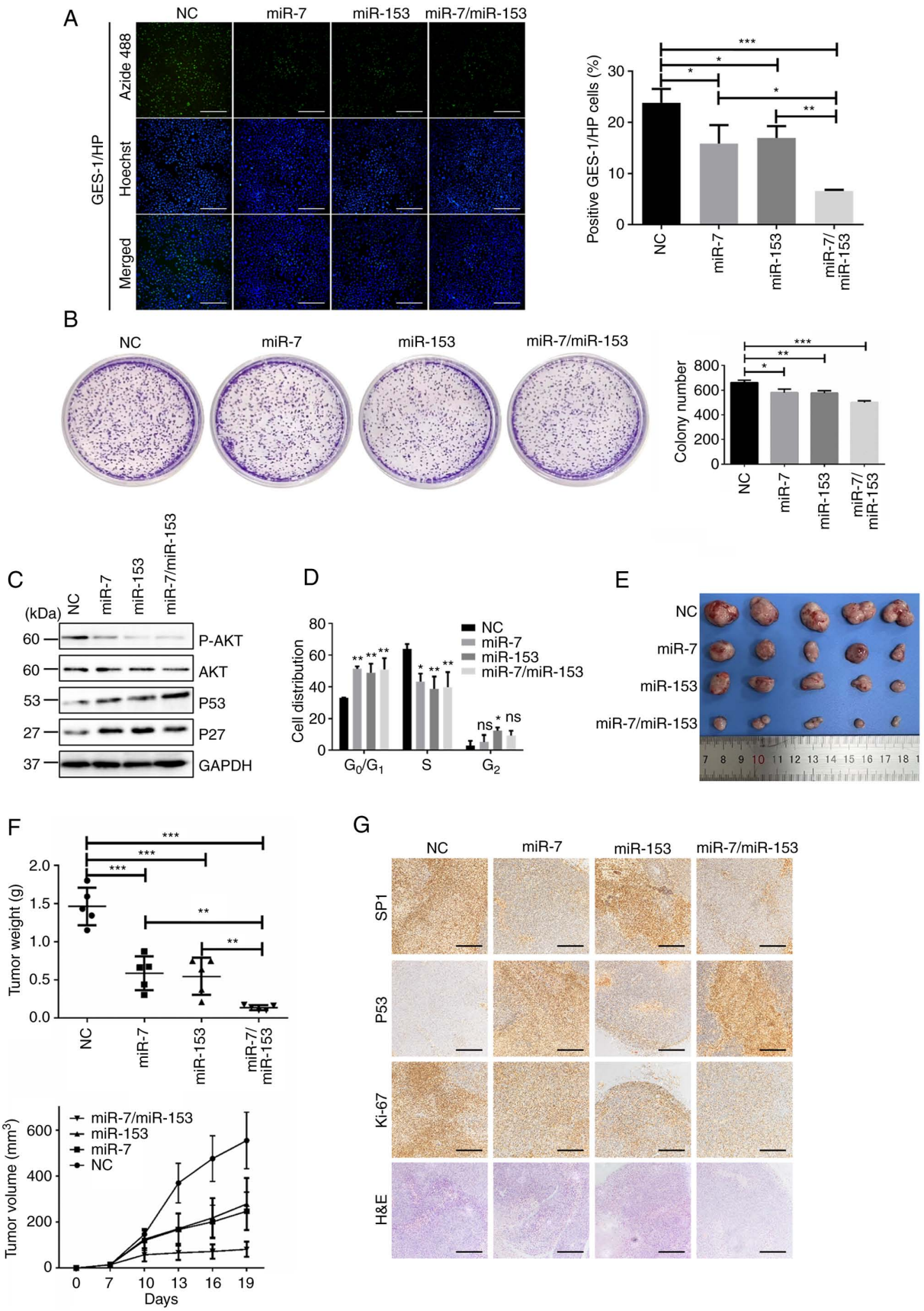

Figure 3. miR-7 and miR-153 combination obviously represses the proliferation of *H. pylori*-associated GC cells. (A) Representative images illustrating the EdU and Hoechst staining of GES-1/HP cells transfected with NC, miR-7 or/and miR-153 (left) and analysis of EdU-positive GES-1/HP cells by and EdU incorporation assay (right). Scale bar, 500 μm, *P<0.05, **P<0.01. (B) Clone formation assay. *P<0.05, **P<0.01, ***P<0.001. (C) Western blot analysis of cell proliferation. (D) Analysis of cell cycle in GES-1/HP cell overexpressed with miR-7 or/and miR-153. *P<0.05, ***P<0.001. (E) Isolated tumors of xenograft models. (F) Tumor weights for various groups are shown on upper panel. **P<0.01, ***P<0.001. Tumor growth curve are displayed on lower panel. (G) Representative immunohistochemical images of subcutaneous tumors of SP1, P53 and Ki-67. Scale bar, 500 μm. miR, microRNA; *H. pylori*, *Helicobacter pylori*; GC, gastric cancer; NC, negative control; H&E, hematoxylin and eosin.

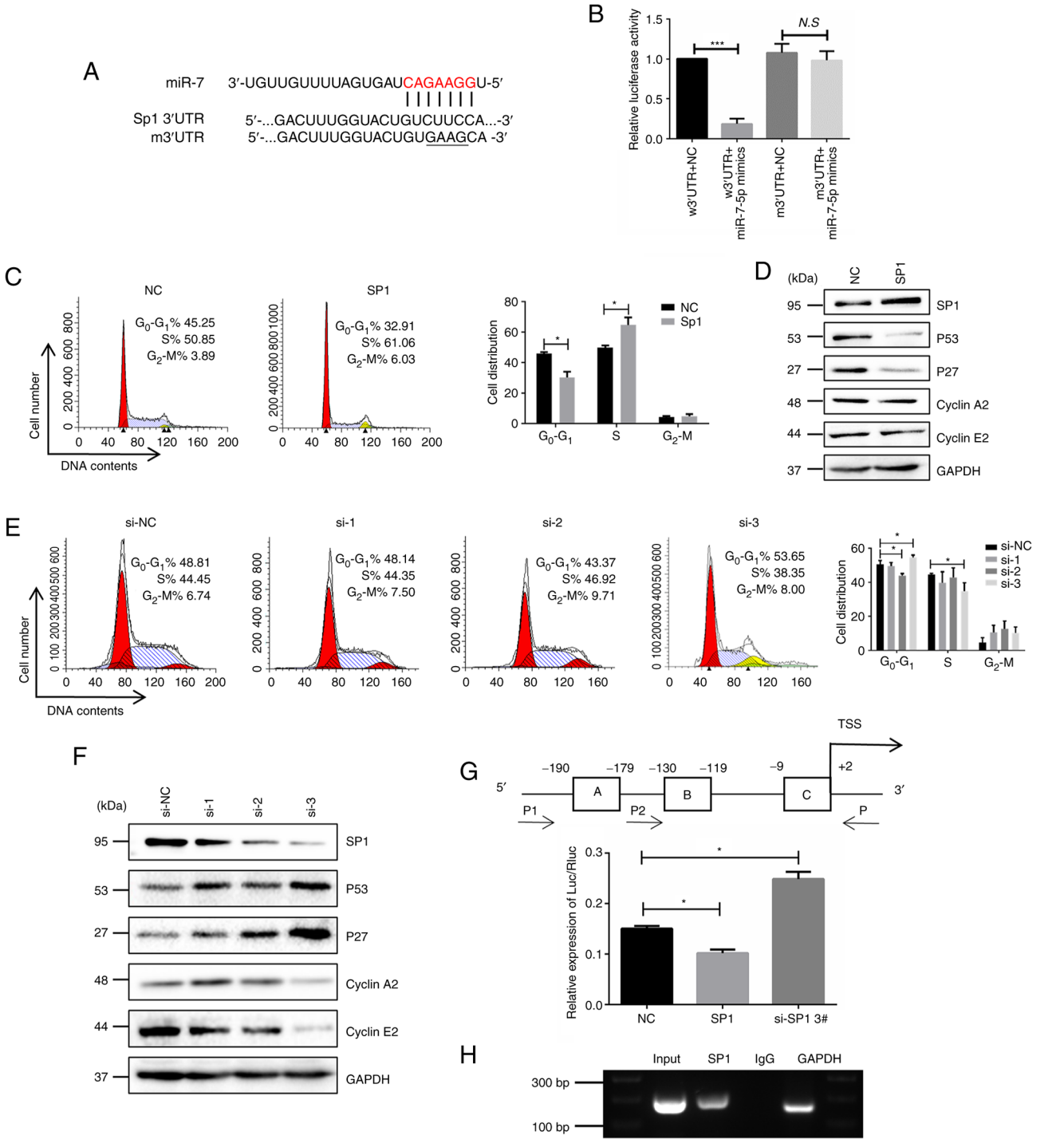

Figure 4. miR-7 induces cell cycle arrest in *H. pylori*-associated GC cells via the Sp1/p53 axis. (A) Putative miR-7 binding sites on 3'-UTR of SP1 and the site discrepancies between wild-type and mutant type (B) GES-1/HP cells co-transfected with miR-7 mimic or mimic-NC and constructed reporter plasmids and relative luciferase activities were detected. ***P<0.001, NS, not significant. (C) Detection of the cell cycle when SP1 was overexpressed in GES-1 cells. *P<0.05. (D) Cell cycle-associated proteins were detected in SP1-overexpressed GES-1 cells. (E) Detection of the cell cycle when SP1 was knockdown in GES-1/HP cells. *P<0.05. (F) Cell cycle-associated proteins were analyzed when SP1 was knockdown in GES-1/HP cells. (G) Upper: Schematic of the partial P53 promoter predicted by Jaspar, three ChIP PCR primers (A-C) and the TSS. Lower: Dual-luciferase reporter assay was performed in GES-1/HP cells when SP1 was overexpressed or knocked down. *P<0.05. (H) ChIP PCR results. miR, microRNA; *H. pylori*, *Helicobacter pylori*; GC, gastric cancer; NC, negative control; ChIP, chromatin immunoprecipitation; TSS, transcription start site.

(Fig. 4B). These results proved that sp1 was a direct target of miR-7 in *H. pylori*-associated GC cells.

Considering the puzzling interplay between p53 and Sp1, Sp1 was overexpressed in GES-1 cell and Sp1-siRNA was adopted in GES-1/HP cells. Cell cycle analysis showed that SP1 is mainly involved in the G_1 phase of the cell cycle (Fig. 4C and D). Western blotting showed that overexpression of Sp1 downregulated the expression of P53 and P27. Nevertheless, P53 and P27 were increased with Sp1 knockdown (Fig. 4D-F). Further promoter analysis showed three putative binding sites of SP1 in the approximate transcription start site of P53 (Fig. 4H). Dual luciferase reporter gene assay

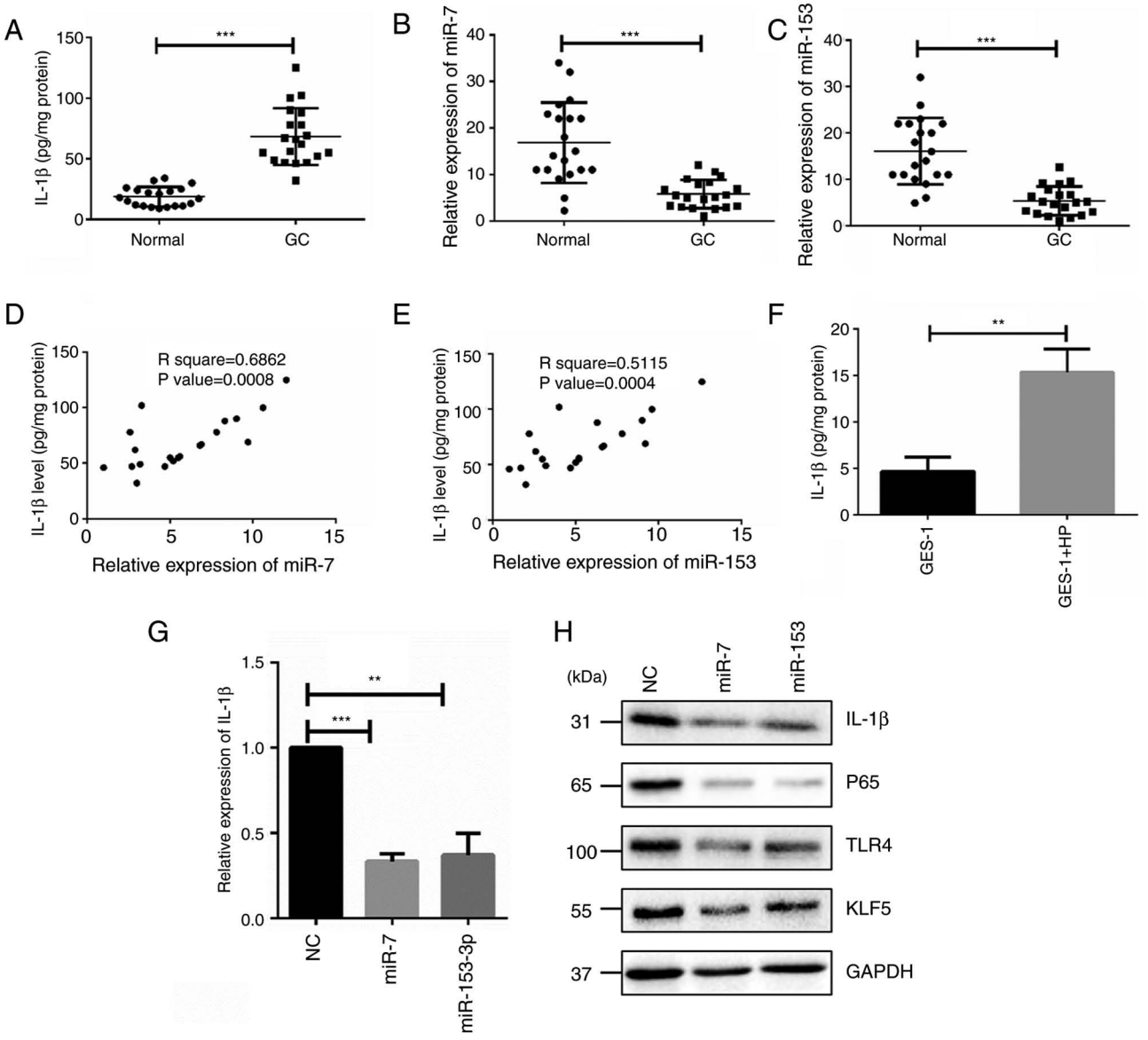

Figure 5. miR-7 and miR-153 regulates NF-kB-induced inflammation via TLR4 and KLF5. (A) Detection of IL-1β between GC and adjacent normal biopsy tissues. ***P<0.001. (B) Detection of miR-7 in GC and adjacent normal biopsy tissues by RT-qPCR. ***P<0.001. (C) Detection of miR-153 in GC and adjacent normal biopsy tissues by RT-qPCR. ***P<0.001. (D) Pearson analysis between IL-1β and expression of miR-7. (E) Pearson analysis between IL-1β and expression of miR-153. (F) Detection of IL-1β with *H. pylori* infection in GES-1 cells. **P<0.01. (G) Detection of IL-1β in GES-1/HP cells overexpressing miR-7 or miR-153. **P<0.01, ***P<0.001. (H) Effect of miR-7 or miR-153 on expression of IL-1β, P65, TLR4 and KLF5 in GES-1/HP cells by western blotting. miR, microRNA; TLR4, Toll-like receptor 4; KLF, Krüppel-like factor; GC, gastric cancer; RT-qPCR, reverse transcription-quantitative PCR; *H. pylori*, *Helicobacter pylori*.

showed that SP1 overexpression significantly reduced the relative luciferase activity, while the relative luciferase activity was enhanced with SP1 knockdown (Fig. 4G). In addition, the ChIP assay showed that SP1 could directly bind to the P53 promoter region. All the findings suggested that cell cycle arrest was enhanced via the Sp1/p53 axis when miR-7 was overexpressed in *H. pylori*-associated GC cells.

miR-7 and miR-153 regulates NF-kB-induced inflammation via TLR4 and KLF5/IL-1β. Some evidence shows an association between IL-1β gene polymorphisms and *H. pylori* infection (38). Meanwhile, the results of the present study also showed that expression of miR-7 and miR-153 were decreased with *H. pylori* infection. To further uncover whether miR-7 and miR-153 control the activity of IL-1β-mediated NF-kB signaling pathway, the present study assessed the IL-1β levels in biopsy specimens obtained from the antrum of gastric patients with *H. pylori* infection and matched normal tissues. ELISA results showed that IL-1β was significantly enhanced in patients with *H. pylori* infection (Fig. 5A). Same samples were used to analyze the expression of miR-7 and miR-153. The RT-qPCR results showed that miR-7 and miR-153 were weakened with *H. pylori* infection (Fig. 5B and C). Furthermore, Pearson correlation analysis showed that the expression of miR-7 or miR-153 was negatively associated with the expression of IL-1β in *H. pylori*-infected GC specimens (Fig. 5D and E). Upregulation of IL-1β level was also detected when GES-1 cells were treated with *H. pylori*

infection (Fig. 5F). Moreover, IL-1β was significantly reduced at both mRNA and protein levels when miR-7 and miR-153 were overexpressed in GES-1/HP cells (Fig. 5E and F). Meanwhile, TLR4 and KLF5 were decreased (Fig. 5H), which is consistent with previous reports, implying that miR-7 and miR-153 regulate NF-kB-induced inflammation via TLR4 and KLF5.

Potentially diagnostic value of miR-7 and miR-153 in H. pylori-associated gastric GC. To investigate the correlation between the expression of miR-7 and miR-153 levels and clinicopathological features of *H. pylori*-associated GC patients, 60 tissue specimens were adopted to analyze the clinical correlation. It was found that low expression of miR-7 and miR-153 was significantly associated with the TNM stage and lymph node metastasis (Table SII). Moreover, the expression changes of miR-7, miR-153, Bcl-xL, SP1 and Bcl2 were analyzed in 20 cases of GC tissues and paired adjacent normal tissues. Downregulation of miR-7 and miR-153 and upregulation of Bcl-xL, Sp1 and Bcl2 were found in GC tissues (Fig. 6A and B). Associations between miR-7, miR-153 and their target Bcl-xL, SP1 and Bcl2 were further confirmed by FISH and ISH analysis on tissue microarray (Fig. 6C).

As shown in Fig. 6D, the area under the curve (AUC) value for combined detection of miR-7 and miR-153 (AUC=0.9675, 95% Confidence Interval (CI): 0.9192-1.106) indicated a higher sensitivity and specificity than miR-7 (AUC=0.9675, 95% CI: 0.8019-0.9981) or miR-153 (AUC=0.9325, 95% CI: 0.8598-1.005) alone in GC tissues. Furthermore, based on the critical role of H. pylori in the carcinogenesis pattern 'chronic gastritis-gastric mucosa atrophy-intestinal metaplasia-dysplasia-gastric cancer', GC tissues from different phases of patients and paired adjacent normal tissues were obtained by endoscopic biopsy or surgical samples and the expression of miR-7 and miR-153 was detected. Results showed that miR-7 and miR-153 were gradually decreased in the process of carcinogenesis (Fig. 6E).

Finally, both miR-7 and miR-153 were detected in serum between healthy individuals and GC patients with *H. pylori* infection. The results showed that miR-7 and miR-153 were significantly downregulated (Fig. 6F and G) and the AUC value for combined detection of miR-7 and miR-153 (AUC=0.9500, 95% CI: 0.8788-1.021) also indicated a higher sensitivity and specificity than miR-7 (AUC=0.8750, 95% CI: 0.7493-1.001) or miR-153 (AUC=0.7800, 95% CI: 0.5823-0.9777) alone in GC serum (Fig. 6H). Collectively, the results showed the potential diagnostic value of miR-7 and miR-153 in *H. pylori*-associated gastric GC.

Discussion

H. pylori is considered a class I carcinogen and an inducer of the long-term evolution of gastric tissue from malignant precancerous lesions to GC (39). Growing evidence has shown the interaction between *H. pylori* infection and dysregulation of miRNA expression (40-42). In the present study, a total of 331 miRNAs were identified as abnormal expression between *H. pylori*-infected GC tissues and compared adjacent normal tissues. Among them, a number of miRNAs have been identified as possessing an association with *H. pylori*-induced gastric carcinogenesis. For example, miR-375 is downregulated in *H. pylori*-induced GC (43), it can inhibit *H. pylori*-induced gastric carcinogenesis by blocking JAK2-STAT3 signaling (44) and reduce the stemness of GC cells through triggering ferroptosis (45); miR-196a-5p is increased in *H. pylori*-positive GC tissue (13,46). In the present study, miR-153 and miR-7 were both downregulated with infection of *H. pylori* and demonstrated to be associated with the virulence factor CagA. Further analysis showed that downregulation of miR-7 and miR-153 can be detected in both serums and clinical tissues of *H. pylori*-associated patients with GC and has been associated with the TNM stage and lymph node metastasis; therefore, conjoint analysis of miR-7 and miR-153 might serve as potential candidate marker in early diagnosis of *H. pylori*-associated GC.

Bcl-2 families have essential roles in apoptotic regulation and have garnered interest as therapeutic targets. The present study identified that Bcl-xL is the target gene of miR-7 and Bcl2 is the target gene of miR-153. Particularly, the combined application of miR-7 and miR-153 can significantly enhance the apoptosis of GES-1/HP cells. Growing evidence has shown that Bcl2 is target of miR-7 in different cancer cells (47,48). However, there was no obvious change on the expression of Bcl2 when miR-7 was overexpressed in GES-1/HP cells, consistent with the previous result of genome-wide screenings (23). It was hypothesized that there is cell specificity. In addition, Bcl2 has been reported to be the target of miR-153 in human glioma (49), colorectal cancer (50) and chronic myeloid leukemia cells (51). The results of the present study confirmed that Bcl2 also can be negative-regulated by miR-153 in GES-1/HP cells.

Previous studies have shown that there is negative association between miR-7 and SP1 and that the miR-7/SP1 axis exerts pivotal roles via different downstream pathways. The miR-7/SP1/TP53BP1 axis may serve a key role in the radiosensitivity of non-small cell lung cancer (52) and miR-7/SP1 axis acts as an effector of MTA2 to affect KLK10 levels and mobility of cervical cancer cells (53). The present study showed that SP1 also can be repressed in miR-7-overexpressed GES-1/HP cells and cell proliferation was significantly attenuated via P53-mediated cell cycle arrest. Previous studies show that there is a puzzling interplay between p53 and Sp1. As transcription factors, both p53 and Sp1 regulate critical cellular life and death decisions. Intriguingly, p53 and Sp1 have similar consensus sequences on GC-boxes and may compete in binding to specific promoters and act in opposite directions (54,55). Li *et al* (56) report that Sp1 is a crucial factor for p53-mediated apoptosis but not cell cycle arrest, which conflicts with the presumed function of Sp1 as an oncogene. The present study showed that SP1 can repress the expression of P53 by directly binding to the promoter of p53.

Studies have shown the connection between inflammation and cancer (57,58). IL-1β, one of the inflammatory factors, is a potent pro-inflammatory cytokine and has been associated with an increased risk of gastritis and non-cardia GC (59). The present study confirmed its obvious elevation in GC with *H. pylori* infection (Fig. 5A). TLR4 has reported to possess a role in the host response to *H. pylori* infection (60,61),

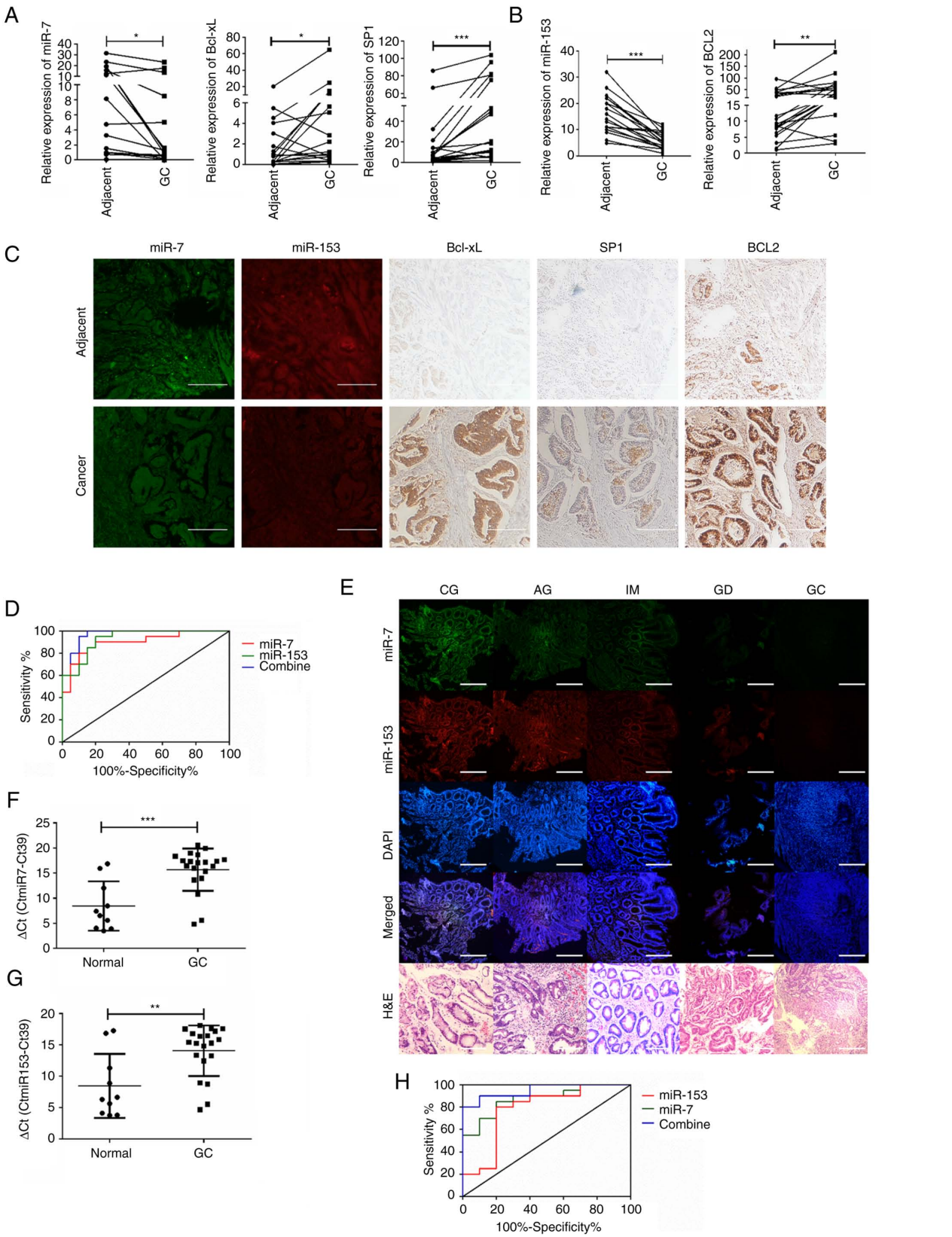

Figure 6. Potentially diagnostic value of miR-7 and miR-153 in *H. pylori*-associated gastric GC. (A) Detection of miR-7 and its targets between GC and adjacent normal tissues. *P<0.05. (B) Detection of miR-153 and its targets between GC and adjacent normal tissues. *P<0.05. (C) Differences of miR-7, miR-153 and their targets were confirmed with FISH and IHC between GC and adjacent normal tissues. Scale bar, 200 μm. (D) Diagnostic efficacy of miR-7, miR-153 and their combine in GC tissues. ROC was introduced for assessing the diagnostic efficacy of miR-7, miR-153 and their combine in GC tissues. GC tissues vs. normal tissues. (E) Differential expressions of miR-7 and miR-153 were detected in GC progression by FISH. Scale bar, 500 μm. (F and G) Detection of miR-7 and miR-153 in serum samples between GC patients and health control. n=10 in normal group and n=20 in GC group; **P<0.05, ***P<0.001. (H) Diagnostic efficacy of miR-7, miR-153 and their combine in GC patient serum. ROC is introduced for assessing the diagnostic efficacy of miR-7, miR-153 and their combination in GC patient serum. GC patient serum vs. normal serum. miR, microRNA; *H. pylori*, *Helicobacter pylori*; GC, gastric cancer; miR, microRNA; TLR4, Toll-like receptor 4; KLF, Krüppel-like factor; FISH, fluorescence *in situ* hybridization; IHC immunohistochemical; ROC, receiver operating characteristic curve; CG, chronic gastritis; AG, atrophic gastritis; IM, intestinal metaplasia; GD, gastric dysplasia.

KLF5 expression is also significantly upregulated following co-culture of *H. pylori* (62). TLR4 and KLF5 are both involved in IL-1β activated NF-κB cascade (63,64). In the present study, overexpression of miR-7 and miR-153 inhibited the expression of NF-κB, miR-7 downregulated TLR4 and miR-153 decreased the expression of KLF5 in accordance with previous studies (65,66).

In conclusion, the present study uncovered a more comprehensive understanding of miR-7 and miR-153 in apoptosis, proliferation and inflammation of *H. pylori*-associated GC cells and provided insights into miR-7 and miR-153 as potential diagnostic marker of GC. Furthermore, its findings suggested that miR-7 and miR-153-targeted therapeutics may represent a potential strategy for *H. pylori* CagA-associated gastric cancer.

Acknowledgements

The authors are grateful to Professor Boqing Li of Binzhou Medical University (Yantai, China) for *H. pylori* strain ATCC 26695 and its corresponding CagA-knockout strain.

Funding

The present study was funded by the National Natural Science Foundation of China (grant no. 82102398), Shandong Provincial Natural Science Foundation (grant nos. ZR2020QC073, ZR2021MH409 and ZR2020MH296), Shandong Province Medical and Health Science and Technology Development Plan (grant nos. 2018WS106 and 202211000314) and the Incubation Project of Weihai Municipal Hospital (grant nos. FH-2021-XZ02 andFH-2021-JY16).

Availability of data and materials

The datasets used during the present study are available from the corresponding author upon reasonable request. The raw data sequencing data from this study have been deposited in the National Genomics Data Center, China National Center for Bioinformation/Beijing Institute of Genomics Chinese Academy of Sciences repository (https://ngdc.cncb.ac.cn/gas-human/; accession no. HRA003675).

Authors' contributions

YS, DG, JFL, LNG, PL, YMQ, HYC, TL, XC, LYS and YRW designed and performed experiments, analyzed data, interpreted results and prepared the manuscript. ZJD helped with designing experiments and evaluating the manuscript. MYW designed experiments, analyzed data and wrote the manuscript. DG, LYS and XC revised the manuscript. MYW and PL confirm the authenticity of all the raw data. All authors read and approved the final manuscript.

Ethics approval and consent to participate

The studies involving human participants were reviewed and approved by the Ethics Committee of Weihai Municipal Hospital (approval no. 2021021). Informed consent to be included in the study was obtained from all patients.

Patient consent of publication

Not applicable.

Competing interests

The authors declare that they have no competing interests.

References

1. Smyth EC, Nilsson M, Grabsch HI, van Grieken NC and Lordick F: Gastric cancer. Lancet 396: 635-648, 2020.
2. Plummer M, Franceschi S, Vignat J, Forman D and de Martel C: Global burden of gastric cancer attributable to *Helicobacter pylori*. Int J Cancer 136: 487-490, 2015.
3. Wen S and Moss SF: *Helicobacter pylori* virulence factors in gastric carcinogenesis. Cancer Lett 282: 1-8, 2009.
4. Nejati S, Karkhah A, Darvish H, Validi M, Ebrahimpour S and Nouri HR: Influence of *Helicobacter pylori* virulence factors CagA and VacA on pathogenesis of gastrointestinal disorders. Microb Pathog 117: 43-48, 2018.
5. Javed S, Skoog EC and Solnick JV: Impact of *Helicobacter pylori* virulence factors on the host immune response and gastric pathology. Curr Top Microbiol Immunol 421: 21-52, 2019.
6. Takahashi-Kanemitsu A, Knight CT and Hatakeyama M: Molecular anatomy and pathogenic actions of *Helicobacter pylori* CagA that underpin gastric carcinogenesis. Cell Mol Immunol 17: 50-63, 2020.
7. Gao S, Song D, Liu Y, Yan H and Chen X: *Helicobacter pylori* CagA PROTEIN ATTENUates 5-Fu sensitivity of gastric cancer cells through upregulating cellular glucose metabolism. Onco Targets Ther 13: 6339-6349, 2020.
8. Lujambio A and Lowe SW: The microcosmos of cancer. Nature 482: 347-355, 2012.
9. Bartel DP: MicroRNAs: Target recognition and regulatory functions. Cell 136: 215-233, 2009.
10. Dastmalchi N, Safaralizadeh R and Banan Khojasteh SM: The correlation between microRNAs and *Helicobacter pylori* in gastric cancer. Pathog Dis 77: ftz039, 2019.
11. Parizadeh SM, Jafarzadeh-Esfehani R, Avan A, Ghandehari M, Goldani F and Parizadeh SM: The prognostic and predictive value of microRNAs in patients with *H. pylori*-positive gastric cancer. Curr Pharm Des 24: 4639-4645, 2018.
12. Zou D, Xu L, Li H, Ma Y, Gong Y, Guo T, Jing Z, Xu X and Zhang Y: Role of abnormal microRNA expression in *Helicobacter pylori* associated gastric cancer. Crit Rev Microbiol 45: 239-251, 2019.
13. Blosse A, Levy M, Robe C, Staedel C, Copie-Bergman C and Lehours P: Deregulation of miRNA in *Helicobacter pylori*-induced gastric MALT lymphoma: From mice to human. J Clin Med 8: 845, 2019.
14. Korać P, Antica M and Matulić M: MiR-7 in cancer development. Biomedicines 9: 325, 2021.
15. Xiao H: MiR-7-5p suppresses tumor metastasis of non-small cell lung cancer by targeting NOVA2. Cell Mol Biol Lett 24: 60, 2019.
16. Xia J, Cao T, Ma C, Shi Y, Sun Y, Wang ZP and Ma J: miR-7 suppresses tumor progression by directly targeting MAP3K9 in pancreatic cancer. Mol Ther Nucleic Acids 13: 121-132, 2018.
17. Li M, Pan M, Wang J, You C, Zhao F, Zheng D, Guo M, Xu H, Wu D, Wang L and Dou J: miR-7 reduces breast cancer stem cell metastasis via inhibiting RELA to decrease ESAM expression. Mol Ther Oncolytics 18: 70-82, 2020.
18. Kong D, Piao YS, Yamashita S, Oshima H, Oguma K, Fushida S, Fujimura T, Minamoto T, Seno H, Yamada Y, *et al*: Inflammation-induced repression of tumor suppressor miR-7 in gastric tumor cells. Oncogene 31: 3949-3960, 2012.
19. Lin J, Liu Z, Liao S, Li E, Wu X and Zeng W: Elevated microRNA-7 inhibits proliferation and tumor angiogenesis and promotes apoptosis of gastric cancer cells via repression of Raf-1. Cell Cycle 19: 2496-2508, 2020.
20. Xu N, Lian YJ, Dai X and Wang YJ: miR-7 increases cisplatin sensitivity of gastric cancer cells through suppressing mTOR. Technol Cancer Res Treat 16: 1022-1030, 2017.
21. Xie J, Chen M, Zhou J, Mo MS, Zhu LH, Liu YP, Gui QJ, Zhang L and Li GQ: miR-7 inhibits the invasion and metastasis of gastric cancer cells by suppressing epidermal growth factor receptor expression. Oncol Rep 31: 1715-1722, 2014.
22. Zhao X, Dou W, He L, Liang S, Tie J, Liu C, Li T, Lu Y, Mo P, Shi Y, *et al*: MicroRNA-7 functions as an anti-metastatic microRNA in gastric cancer by targeting insulin-like growth factor-1 receptor. Oncogene 32: 1363-1372, 2013.

23. Zhao XD, Lu YY, Guo H, Xie HH, He LJ, Shen GF, Zhou JF, Li T, Hu SJ, Zhou L, *et al*: MicroRNA-7/NF-κB signaling regulatory feedback circuit regulates gastric carcinogenesis. J Cell Biol 210: 613-627, 2015.
24. Ye T, Yang M, Huang D, Wang X, Xue B, Tian N, Xu X, Bao L, Hu H, Lv T and Huang Y: MicroRNA-7 as a potential therapeutic target for aberrant NF-κB-driven distant metastasis of gastric cancer. J Exp Clin Cancer Res 38: 55, 2019.
25. Wang L, Lv X, Fu X, Su L, Yang T and Xu P: MiR-153 inhibits the resistance of lung cancer to gefitinib via modulating expression of ABCE1. Cancer Biomark 25: 361-369, 2019.
26. Shi D, Li Y, Fan L, Zhao Q, Tan B and Cui G: Upregulation of miR-153 inhibits triple-negative breast cancer progression by targeting ZEB2-mediated EMT and contributes to better prognosis. Onco Targets Ther 12: 9611-9625, 2019.
27. Li C, Zhang Y, Zhao W, Cui S and Song Y: miR-153-3p regulates progression of ovarian carcinoma in vitro and in vivo by targeting MCL1 gene. J Cell Biochem 120: 19147-19158, 2019.
28. Zhang W, Mao S, Shi D, Zhang J, Zhang Z, Guo Y, Wu Y, Wang R, Wang L, Huang Y and Yao X: MicroRNA-153 decreases tryptophan catabolism and inhibits angiogenesis in bladder cancer by targeting indoleamine 2,3-dioxygenase 1. Front Oncol 9: 619, 2019.
29. Bi CW, Zhang GY, Bai Y, Zhao B and Yang H: Increased expression of miR-153 predicts poor prognosis for patients with prostate cancer. Medicine (Baltimore) 98: e16705, 2019.
30. Zhang L, Pickard K, Jenei V, Bullock MD, Bruce A, Mitter R, Kelly G, Paraskeva C, Strefford J, Primrose J, *et al*: miR-153 supports colorectal cancer progression via pleiotropic effects that enhance invasion and chemotherapeutic resistance. Cancer Res 73: 6435-6447, 2013.
31. Ouyang Y, Yuan W and Qiu S: MicroRNA-153 functions as a tumor suppressor in gastric cancer via targeting Kruppel-like factor 5. Exp Ther Med 16: 473-482, 2018.
32. Guo Y, Zhang T, Shi Y, Zhang J, Li M, Lu F, Zhang J, Chen X and Ding S: *Helicobacter pylori* inhibits GKN1 expression via the CagA/p-ERK/AUF1 pathway. Helicobacter 25: e12665, 2020.
33. Liu JF, Guo D, Kang EM, Wang YS, Gao XZ, Cong HY, Liu P, Zhang NQ and Wang MY: Acute and chronic infection of *H. pylori* caused the difference in apoptosis of gastric epithelial cells. Microb Pathog 150: 104717, 2021.
34. Livak KJ and Schmittgen TD: Analysis of relative gene expression data using real-time quantitative PCR and the 2(-Delta Delta C(T)) method. Methods 25: 402-408, 2001.
35. Hayashi Y, Tsujii M, Wang J, Kondo J, Akasaka T, Jin Y, Li W, Nakamura T, Nishida T, Iijima H, *et al*: CagA mediates epigenetic regulation to attenuate let-7 expression in *Helicobacter pylori*-related carcinogenesis. Gut 62: 1536-1546, 2013.
36. Yuan J, Li Y, Liao J, Liu M, Zhu L and Liao K: MicroRNA-7 inhibits hepatocellular carcinoma cell invasion and metastasis by regulating Atg5-mediated autophagy. Transl Cancer Res 9: 3965-3972, 2020.
37. Hou S, Guo M, Xi H, Zhang L, Zhao A, Hou H and Fang W: MicroRNA-153-3p sensitizes melanoma cells to dacarbazine by suppressing ATG5-mediated autophagy and apoptosis. Transl Cancer Res 9: 5626-5636, 2020.
38. Ren HY, Wen LS, Geng YH, Huang JB, Liu JF, Shen DY and Meng JR: Association between IL-1B gene polymorphisms and *Helicobacter pylori* infection: A meta-analysis. Microb Pathog 137: 103769, 2019.
39. Wang F, Meng W, Wang B and Qiao L: *Helicobacter pylori*-induced gastric inflammation and gastric cancer. Cancer Lett 345: 196-202, 2014.
40. Han T, Jing X, Bao J, Zhao L, Zhang A, Miao R, Guo H, Zhou B, Zhang S, Sun J and Shi J: *H. pylori* infection alters repair of DNA double-strand breaks via SNHG17. J Clin Invest 130: 3901-3918, 2020.
41. So JBY, Kapoor R, Zhu F, Koh C, Zhou L, Zou R, Tang YC, Goo PCK, Rha SY, Chung HC, *et al*: Development and validation of a serum microRNA biomarker panel for detecting gastric cancer in a high-risk population. Gut 70: 829-837, 2021.
42. Liu Y, Zhu J, Ma X, Han S, Xiao D, Jia Y and Wang Y: ceRNA network construction and comparison of gastric cancer with or without *Helicobacter pylori* infection. J Cell Physiol 234: 7128-7140, 2019.
43. Zhang Z, Chen S, Fan M, Ruan G, Xi T, Zheng L, Guo L, Ye F and Xing Y: *Helicobacter pylori* induces gastric cancer via down-regulating miR-375 to inhibit dendritic cell maturation. Helicobacter 26: e12813, 2021.
44. Miao L, Liu K, Xie M, Xing Y and Xi T: miR-375 inhibits *Helicobacter pylori*-induced gastric carcinogenesis by blocking JAK2-STAT3 signaling. Cancer Immunol Immunother 63: 699-711, 2014.
45. Ni H, Qin H, Sun C, Liu Y, Ruan G, Guo Q, Xi T, Xing Y and Zheng L: MiR-375 reduces the stemness of gastric cancer cells through triggering ferroptosis. Stem Cell Res Ther 12: 325, 2021.
46. Lee JW, Kim N, Park JH, Kim HJ, Chang H, Kim JM, Kim JW and Lee DH: Differential MicroRNA expression between gastric cancer tissue and non-cancerous gastric mucosa according to *Helicobacter pylori* status. J Cancer Prev 22: 33-39, 2017.
47. Hong T, Ding J and Li W: miR-7 reverses breast cancer resistance to chemotherapy by targeting MRP1 And BCL2. Onco Targets Ther 12: 11097-11105, 2019.
48. Xiong S, Zheng Y, Jiang P, Liu R, Liu X and Chu Y: MicroRNA-7 inhibits the growth of human non-small cell lung cancer A549 cells through targeting BCL-2. Int J Biol Sci 7: 805-814, 2011.
49. Sun D, Mu Y and Piao H: MicroRNA-153-3p enhances cell radiosensitivity by targeting BCL2 in human glioma. Biol Res 51: 56, 2018.
50. He Y, Zhang L, Tan F, Wang LF, Liu DH, Wang RJ and Yin XZ: MiR-153-5p promotes sensibility of colorectal cancer cells to oxaliplatin via targeting Bcl-2-mediated autophagy pathway. Biosci Biotechnol Biochem 84: 1645-1651, 2020.
51. Li YL, Tang JM, Chen XY, Luo B, Liang GH, Qu Q and Lu ZY: MicroRNA-153-3p enhances the sensitivity of chronic myeloid leukemia cells to imatinib by inhibiting B-cell lymphoma-2-mediated autophagy. Hum Cell 33: 610-618, 2020.
52. Guo G, Li L, Song G, Wang J, Yan Y and Zhao Y: miR-7/SP1/TP53BP1 axis may play a pivotal role in NSCLC radiosensitivity. Oncol Rep 44: 2678-2690, 2020.
53. Lin CL, Ying TH, Yang SF, Wang SW, Cheng SP, Lee JJ and Hsieh YH: Transcriptional suppression of miR-7 by MTA2 induces Sp1-mediated KLK10 expression and metastasis of cervical cancer. Mol Ther Nucleic Acids 20: 699-710, 2020.
54. Wang MJ, Pei DS, Qian GW, Yin XX, Cheng Q, Li LT, Li HZ and Zheng JN: p53 regulates Ki-67 promoter activity through p53- and Sp1-dependent manner in HeLa cells. Tumour Biol 32: 905-912, 2011.
55. Drayman N, Ben-Nun-Shaul O, Butin-Israeli V, Srivastava R, Rubinstein AM, Mock CS, Elyada E, Ben-Neriah Y, Lahav G and Oppenheim A: p53 elevation in human cells halt SV40 infection by inhibiting T-ag expression. Oncotarget 7: 52643-52660, 2016.
56. Li H, Zhang Y, Ströse A, Tedesco D, Gurova K and Selivanova G: Integrated high-throughput analysis identifies Sp1 as a crucial determinant of p53-mediated apoptosis. Cell Death Differ 21: 1493-1502, 2014.
57. Balkwill F and Mantovani A: Inflammation and cancer: Back to Virchow? Lancet 357: 539-545, 2001.
58. Coussens LM and Werb Z: Inflammation and cancer. Nature 420: 860-867, 2002.
59. El-Omar EM, Carrington M, Chow WH, McColl KE, Bream JH, Young HA, Herrera J, Lissowska J, Yuan CC, Rothman N, *et al*: Interleukin-1 polymorphisms associated with increased risk of gastric cancer. Nature 404: 398-402, 2000.
60. Kawahara T, Kuwano Y, Teshima-Kondo S, Kawai T, Nikawa T, Kishi K and Rokutan K: Toll-like receptor 4 regulates gastric pit cell responses to *Helicobacter pylori* infection. J Med Invest 48: 190-197, 2001.
61. Kawahara T, Teshima S, Oka A, Sugiyama T, Kishi K and Rokutan K: Type I *Helicobacter pylori* lipopolysaccharide stimulates toll-like receptor 4 and activates mitogen oxidase 1 in gastric pit cells. Infect Immun 69: 4382-4389, 2001.
62. Noto JM, Khizanishvili T, Chaturvedi R, Piazuelo MB, Romero-Gallo J, Delgado AG, Khurana SS, Sierra JC, Krishna US, Suarez G, *et al*: *Helicobacter pylori* promotes the expression of Krüppel-like factor 5, a mediator of carcinogenesis, in vitro and in vivo. PLoS One 8: e54344, 2013.
63. Xie Z, Jie Z, Wang G, Sun X, Tang P, Chen S, Qin A, Wang J and Fan S: TGF-β synergizes with ML264 to block IL-1β-induced matrix degradation mediated by Krüppel-like factor 5 in the nucleus pulposus. Biochim Biophys Acta Mol Basis Dis 1864: 579-589, 2018.
64. Tang J, Xu L, Zeng Y and Gong F: Effect of gut microbiota on LPS-induced acute lung injury by regulating the TLR4/NF-kB signaling pathway. Int Immunopharmacol 91: 107272, 2021.
65. Zhang XD, Fan QY, Qiu Z and Chen S: MiR-7 alleviates secondary inflammatory response of microglia caused by cerebral hemorrhage through inhibiting TLR4 expression. Eur Rev Med Pharmacol Sci 22: 5597-5604, 2018.
66. Yu L, Xu Q, Yu W, Duan J and Dai G: LncRNA cancer susceptibility candidate 15 accelerates the breast cancer cells progression via miR-153-3p/KLF5 positive feedback loop. Biochem Biophys Res Commun 506: 819-825, 2018.